Chapter 7
The Liutex Shear Interaction in Boundary Layer Transition

Biyu Pang, Yuan Ding, and Yiqian Wang

Abstract The third generation of vortex identification methods based on Liutex vector are superior to previous methods in that they overcome the drawbacks of previous methods including threshold problem, shear contamination, etc. with a clear physical meaning for the Liutex vector. The direction of Liutex represents the local axis of rotation, and its magnitude is equal to twice the angular velocity of rotation. The current study focuses on the interaction between Liutex represented rotation and the residual shear part during the development of Λ vortex and hairpin vortex in boundary layer transition. The results show that shear plays an important role in the generation and dissipation of vortices and the proportion of Liutex in the whole vorticity affects the stability of a vortex. When the directions between Liutex and shear is approximately parallel, the vortex moves mainly along the flow direction and the offsets in other directions are relatively small. It is also shown that the Liutex vector can accurately extract the rigid rotation part from fluid motion and the third-generation vortex identification methods can serve as a powerful tool to study fluid dynamics.

7.1 Introduction

In both nature and industrial applications, vortex structure is everywhere, especially in turbulence. It plays an important role in the study of the generation and maintenance of turbulence. Therefore, a fully understanding and a mathematical definition of vortex with systematical methods to accurately identify the vortex structure are of great significance in understanding the flow mechanism, turbulent structures [1, 2]. So far, there is still no widely accepted vortex definition and identification method. The vorticity-based vortex identification methods, classified as the first generation here, confuse the concepts of vortex and vorticity, and regards the magnitude of vorticity as the intensity of local rotational motion. However, Robinson [3] found that there was a low correlation between the high vorticity region and the actual

B. Pang · Y. Ding · Y. Wang (✉)
School of Mathematical Science, Soochow University, Suzhou 215006, China
e-mail: yiqian@suda.edu.cn

Y. Wang et al. (eds.), *Liutex and Third Generation of Vortex Identification*,
Springer Proceedings in Physics 288, https://doi.org/10.1007/978-981-19-8955-1_7

vortex structure. Therefore, several vortex identification methods based on Cauchy-Stokes decomposition were introduced, here categorized as the second-generation methods. These methods improve the visualization of vortices, but still suffer from some issues. Firstly, the physical meanings of the methods are not clear and different from each other. Secondly, as iso-surface based methods, the problem of threshold selection is introduced. Thirdly, the information of velocity gradient tensor $\nabla \boldsymbol{V}$ is not fully utilized. These problems of traditional vortex identification methods need to be dealt with [4]. The first part of this paper revisits the vortex identification methods, mainly the new introduced third generation of vortex identification methods based on Liutex vector. The second part describes the shear contamination analysis under the Liutex-shear decomposition. In the third part, taking the boundary layer transition as an example, the interaction between Liutex and shear is discussed. The fourth part summarizes the conclusions of current study.

7.2 Vortex Identification Method

To deal with the issues of first and second-generation vortex identification methods, the team led by Professor Chaoqun Liu of the University of Texas at Arlington carried out various research works and proposed vortex identification methods, including Ω vortex identification method, Liutex vector, Ω-Liutex method and so on [4–6]. Liu et al. [5] proposed the Ω vortex identification method to overcome the problem of threshold selection, and further proposed the Liutex vector that can accurately identify the vortex structure. This definition decomposes the vorticity $\boldsymbol{\omega}$ into a rotating part $\boldsymbol{R}$ and a residual pure shear part $\boldsymbol{\omega} - \boldsymbol{R}$. Liutex is a vector whose direction represents the local axis of rotation and whose magnitude represents twice the rotational angular velocity of rigid motion. It not only solves the problem of threshold selection, but also answers the problem of six elements of vortex definition. After that, Dong et al. [7] proposed a new normalized Ω_R vortex identification method.

7.2.1 Vortex, Vorticity, Velocity Gradient Tensor

Broadly speaking, vortex refers to the rotational motion of fluid, and vorticity is defined as the curl of velocity vector (i.e., $\boldsymbol{\omega} = \nabla \times \boldsymbol{V}$). Its physical meaning is not clear. Robinson [3] pointed out that near the wall of the turbulent boundary layer, the correlation between the vorticity concentration area and the actual vortices is rather low. Wang et al. [8] found in the boundary layer transition the Λ vortex has smaller vorticity at the vortex core than that in the surroundings. This shows that vortex and vorticity are different, and vorticity cannot represent the rotational motion of fluid. The pattern of local fluid motion can be derived from the velocity gradient tensor $\nabla \boldsymbol{V}$ [9], and most Eulerian vortex identification methods are dependent on the velocity gradient tensor.

7.2.2 Cauchy-Stokes Decomposition

The first and major second-generation methods are generally based on Cauchy-Stokes decomposition, including vorticity-based vortex identification method, Q method, λ_2 method and Ω method. The most fundamental problem of these methods is that Cauchy-Stokes decomposition cannot represent the decomposition of fluid motion. Generally, Cauchy-Stokes decomposition is understood as twice the angular velocity of rigid rotation of fluid element around its center. However, in practical application, there is a contradiction between the fluid rotation motion based on Cauchy-Stokes decomposition and vorticity. For example, in the two-dimensional simple shear layer, there is a fluid rotation part according to Cauchy-Stokes decomposition, but in fact, there is no rotational motion in the flow field [9].

7.2.3 Velocity Gradient Tensor

The other approach is based on the analysis of the velocity gradient tensor $\nabla \boldsymbol{V}$ itself, including Δ methods and λ_{ci} method. Both of them define vortex as the region where $\nabla \boldsymbol{V}$ has two complex conjugate eigenvalues. They are scalar vortex identification methods, which ignore the information such as the rotation axis of fluid rotation. Q, λ_2, Δ and λ_{ci} methods are fuzzy to represent the rotation intensity of vortex structure, and they are different from each other. In fact, these methods contain varying degrees of shear contamination [9, 10].

7.2.4 Liutex Vector

Liu et al. [6] pointed out that the vorticity should be decomposed into a rotating part and a non-rotating part, and proposed the Liutex vector which can accurately capture the vortex structure. Liutex is a vector that can accurately describe the local rigid rotational motion of the fluid. The definition of Liutex vector can be summarized as follows.

7.2.4.1 Direction of Liutex

In the initial xyz coordinate system, the velocity gradient tensor $\nabla \boldsymbol{V}$ and its eigenvalues are calculated. When $\nabla \boldsymbol{V}$ has a real eigenvalue λ_r and two complex conjugate eigenvalues $\lambda_{cr} \pm i\lambda_{ci}$, there would only tension or compression in the direction of the real eigenvector $\boldsymbol{v}_r$ corresponding to the real eigenvalue λ_r, and there is no rotational motion in this direction. The rotational motion can only occur in the plane perpendicular to the real eigenvector $\boldsymbol{v}_r$, that is, $\boldsymbol{v}_r$ is the rotation axis of the local fluid

element, The complex conjugate eigenvalues $\lambda_{cr} \pm i\lambda_{ci}$ indicate that the instantaneous streamline presents a circular or spiral shape, that is, there is a vortex structure. The unit direction vector of Liutex vector is $\boldsymbol{r} = \boldsymbol{v}_r$ and we require $\langle \boldsymbol{\omega} \cdot \boldsymbol{v}_r \rangle > 0$.

7.2.4.2 Strength of Liutex

Firstly, **Q** rotation is used to rotate the initial xyz coordinate system to $x_Q y_Q z_Q$, so that the rotated z_Q is in the same direction as the rotation axis $\boldsymbol{r}$, and the velocity gradient tensor $\nabla \boldsymbol{V_Q}$ after rotation becomes

$$\nabla \boldsymbol{V_Q} = \begin{bmatrix} \frac{\partial u_Q}{\partial x_Q} & \frac{\partial u_Q}{\partial y_Q} & 0 \\ \frac{\partial v_Q}{\partial x_Q} & \frac{\partial v_Q}{\partial y_Q} & 0 \\ \frac{\partial w_Q}{\partial x_Q} & \frac{\partial w_Q}{\partial y_Q} & \frac{\partial w_Q}{\partial z_Q} \end{bmatrix} \tag{7.1}$$

$\left(u_Q, v_Q, w_Q\right)$ is the velocity component in $x_Q y_Q z_Q$ coordinate system after **Q** rotation. Here, the formula of Rodrigues is used to solve $\boldsymbol{Q}$. $\boldsymbol{Q}$ is the coordinate rotation matrix. See [4] for specific expressions.

A second rotation (**P** rotation) is used to rotate the reference frame around the z_Q-axis and the corresponding velocity gradient tensor $\nabla \boldsymbol{V_P}$ can be written as

$$\nabla \boldsymbol{V_P} = \boldsymbol{P} \nabla \boldsymbol{V_Q} \boldsymbol{P^T} \tag{7.2}$$

with

$$\nabla \boldsymbol{V_\theta} = \boldsymbol{P_r} \nabla \boldsymbol{V_Q} \boldsymbol{P_r^T} = \begin{bmatrix} \frac{\partial u}{\partial x}\Big|_\theta & \frac{\partial u}{\partial y}\Big|_\theta & 0 \\ \frac{\partial v}{\partial x}\Big|_\theta & \frac{\partial v}{\partial y}\Big|_\theta & 0 \\ \frac{\partial w}{\partial x}\Big|_\theta & \frac{\partial w}{\partial y}\Big|_\theta & \frac{\partial w}{\partial z}\Big|_\theta \end{bmatrix} \tag{7.3}$$

where the rotation matrix $\boldsymbol{P_r}$ is given by

$$\boldsymbol{P_r} = \begin{bmatrix} cos\theta & sin\theta & 0 \\ -sin\theta & cos\theta & 0 \\ 0 & 0 & 1 \end{bmatrix} \tag{7.4}$$

And α and β are defined as [10]

$$\alpha = \frac{1}{2}\sqrt{\left(\frac{\partial v_Q}{\partial y_Q} - \frac{\partial u_Q}{\partial x_Q}\right)^2 + \left(\frac{\partial v_Q}{\partial x_Q} + \frac{\partial u_Q}{\partial y_Q}\right)^2} \tag{7.5}$$

$$\beta = \frac{1}{2}\left(\frac{\partial v_Q}{\partial x_Q} - \frac{\partial u_Q}{\partial y_Q}\right) \tag{7.6}$$

Then, according to Liu et al. [11] the Liutex magnitude/rotational strength is defined as

$$R = \begin{cases} 2(\beta - \alpha), & \alpha^2 - \beta^2 < 0 \\ 0, & \alpha^2 - \beta^2 \geq 0 \end{cases} \tag{7.7}$$

and here we assume $\beta > 0$ (if $\beta < 0$, we can first rotate the local axis to the opposite direction of v_r to make it positive).

7.2.4.3 Explicit Formula for the Liutex Vector

Liutex is a vector defined as $\boldsymbol{R} = R\boldsymbol{r}$, where R is the magnitude of Liutex, and $\boldsymbol{r}$ is the direction of Liutex. $\boldsymbol{r}$ is the normalized real eigenvector of the velocity gradient tensor such that $\boldsymbol{\omega} \cdot \boldsymbol{r} > 0$. From Wang et al. [11] study on the explicit formula for the Liutex vector and physical meaning of vorticity based on the Liutex-Shear decomposition, an explicit formula of the Liutex vector can be derived as

$$\boldsymbol{R} = \left(\boldsymbol{\omega} \cdot \boldsymbol{r} - \sqrt{(\boldsymbol{\omega} \cdot \boldsymbol{r})^2 - 4\lambda_{ci}^2} \right) \boldsymbol{r} \tag{7.8}$$

7.2.4.4 Advantage of Liutex

As the third-generation vortex identification methods, Liutex-based vortex identification system outperforms the previous two generations, as mainly reflected by:

- Liutex vector is an accurate representation of the physical amount of vortex with a clear physical meaning.
- The vortex identification method represented by Liutex solves the problem of threshold selection for the second-generation of vortex identification methods.
- The Liutex method is able to represent quantitatively the six elements of vortex.

7.3 Shear Contamination

According to the concept of Liutex vector, the vorticity is decomposed into rotating part and non-rotating part. The non-rotating part is pure shear. Mathematically, Cauchy-Stokes decomposition is correct, but the physical meaning is not clear and depends on the choice of coordinates. In different coordinate systems, the forms of rotation matrix, tension matrix, shear matrix and deformation matrix generated by

Table 7.1 Contamination by stretching and shearing on different criteria

Methods	Q	Δ	λ_2	λ_{ci}	Liutex
Contamination by stretching	Yes	Yes	Yes	No	No
Contamination by shearing	Yes	Yes	Yes	Yes	No

Source Copy of Table 1, Page 18, Stretching and shearing contamination analysis for Liutex and other vortex identification methods by Pushpa Shrestha et al. [10]

velocity gradient tensor decomposition will also be different, which makes the analysis of pollution uncertain. Shrestha et al. [10] studied the pollution matrix in the principal coordinate system and obtained the theoretical pollution analysis results in the principal coordinate system (see Table 7.1).

7.3.1 Principal Decomposition

Because of the uniqueness of the principal coordinates, we selected the principal coordinates for analysis, i.e., by coordinate rotation so that the new z axis points in the direction of the local axis of rotation and so that the x and y axis are stretched or compressed the same in the plane of rotation.

Definition 1. The Principal Decomposition is the decomposition of velocity gradient tensor under the Principal Coordinates [10] i.e.,

$$\nabla \boldsymbol{V} = \begin{bmatrix} \lambda_{cr} & -\frac{R}{2} & 0 \\ \frac{R}{2}+\varepsilon & \lambda_{cr} & 0 \\ \xi & \eta & \lambda_r \end{bmatrix} = \begin{bmatrix} 0 & -\frac{R}{2} & 0 \\ \frac{R}{2} & 0 & 0 \\ 0 & 0 & 0 \end{bmatrix} + \begin{bmatrix} 0 & 0 & 0 \\ \varepsilon & 0 & 0 \\ \xi & \eta & 0 \end{bmatrix} + \begin{bmatrix} \lambda_{cr} & 0 & 0 \\ 0 & \lambda_{cr} & 0 \\ 0 & 0 & \lambda_r \end{bmatrix}$$

$$= \boldsymbol{R} + \boldsymbol{S} + \boldsymbol{C}$$

Here $\boldsymbol{R}$ represents the rotation part, $\boldsymbol{S}$ represents the shear part, and $\boldsymbol{C}$ represents the stretching and compression part in three axis directions. ε, λ_{cr} and λ_r are components of either the shear part or stretching part, or both [12].

Shrestha et al. [10] studied the influence of shear or tension on different vortex identification methods through theoretical contamination analysis, and the results are shown in Table 7.1.

7.3.2 Shear in Boundary Layer Transition

Boundary layer transition is a transition process from laminar flow to turbulence, during which Λ vortex structure, hairpin vortex and annular vortex are generated. With the emergence of high frequency annular vortex in the outer layer, the flow

near the wall of the boundary layer first appears disorder. The research shows that in the initial stage of flow disorder, the flow disorder is affected by the instability of local high shear layer. Therefore, it is necessary to study the effect of Liutex shear interaction in boundary layer transition [13–17]. In the transition phase, the inflow boundary is disturbed by T-S waves, and the unstable two-dimensional T-S waves develop along the flow direction, and there is only high shear near the wall without rotational motion. As the flow develops downstream, the 2-D T-S waves begin to show spanwise changes from 2-D disturbance to 3-D disturbance, and accompanied by the emergence of spikes and decay. The schematic of flow transition on a flat plan can be described in the Book of Boundary Layer Theory by Schlichting and Gersten [18]. Next, taking the boundary layer transition as an example, we calculate the cosine values of the angle between Liutex and shear by making the inner product of Liutex vector and shear vector. Specific vortices are selected as the research object, and the cosine value change of Λ vortex moving along the flow direction at a certain time, the development and change of hairpin vortex with time are analyzed. Take the position where the inclined angle is approximately 0 as vortex core lines, the trend for percentage of Liutex over vorticity, and the Liutex shear interaction in the process of boundary layer transition are detailed.

7.4 Numerical Study and Observation

In order to study the transition process of flat plate boundary layer, the numerical data satisfying the characteristics of small-scale vortex and chaos are selected to represent the fully developed turbulence. Meyer et al. [19] believe that the chaos is that "the inclined high shear layer between the Λ vortex legs shows an increased phase jitter from its tip to the wall region." The visualization results in the transition process are displayed by carefully observing and analyzing DNS data [20–25].

7.4.1 Case Setup

The grid level is $1280 \times 256 \times 241$, representing the number of grids in streamwise (x), spanwise (y), and wall normal (z) directions. The grid is stretched in the normal direction and uniform in the streamwise and spanwise directions. Here, $x_{in} = 300.792\delta_{in}$ represents the distance between leading edge and inlet, $Lx = 672.021\delta_{in}$, $Ly = 22\delta_{in}$, $Lz_{in} = 40\delta_{in}$ are the lengths of the computational domain in x-, y-, and z-directions, respectively, δ_{in} represents inflow displacement thickness [16].

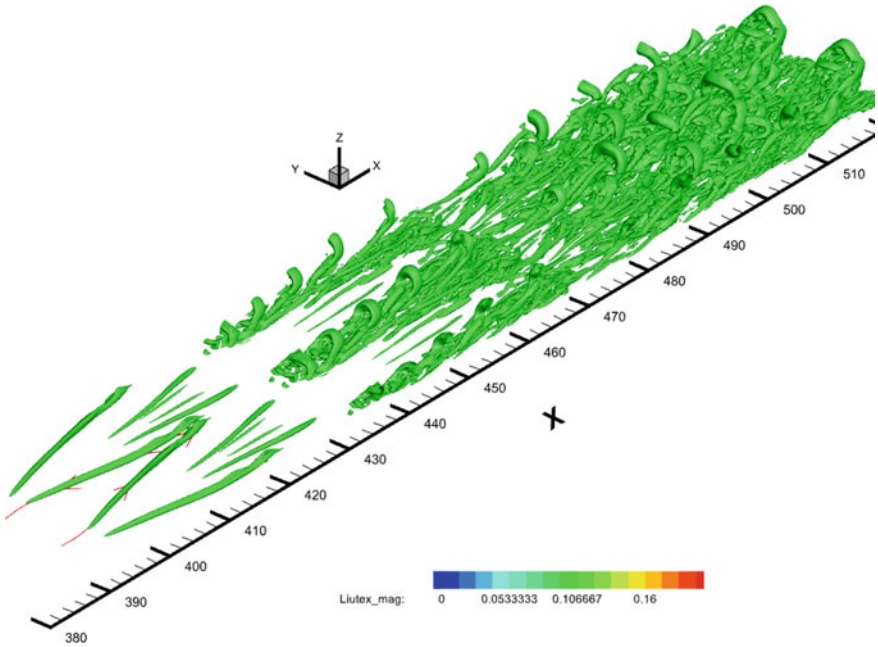

Fig. 7.1 Multiple ring generation and vortex structures

7.4.2 Visualization of Simulation Results

The DNS code "DNSUTA" has been carefully verified by NASA Langley and UTA researchers to ensure that the DNS results are correct and reliable. The following are the visualization results and analysis of the simulation [16].

7.4.2.1 Vortex Structures and Flow Transition

Figure 7.1 shows the visualization of flow transition by an iso-surface of Liutex magnitude equal to 0.1. It includes Λ vortex, hairpin vortex and annular vortex. We can see hairpin structures are pretty clear. In particular, the Liutex lines can accurately describe the structure of vortex. In order to study the role of Liutex and shear in the formation and development of small-scale vortices, we need to pay attention to the location and change information of Liutex and shear.

7.4.2.2 Liutex and Shear Interaction

In the boundary layer transition, two slices $x = 408.98\delta_{in}$ and $y = 10.99\delta_{in}$ are selected, and the point with the largest Liutex magnitude is taken as the seed points

of the Liutex respectively. The $cos\theta$ values of Liutex and shear at the vortex core of Λ vortex and hairpin vortex are calculated and compared.

The structure of Λ vortex and hairpin vortex is shown in Fig. 7.2. Through numerical simulation, we get that the integral average value of $cos\theta$ is 0.723 on the vortex core line in Fig. 7.2a, and the integral average value of $cos\theta$ is 0.962 on the vortex core line in Fig. 7.2b.

Next, we take Λ vortex as the research object and extract the Liutex core line data representing the vortex core, as listed in Table 7.2. The variation of $cos\theta$ values on Liutex core line with flow direction is studied when $t = 5.5T$ (T is the period of T-S wave), as shown in the Fig. 7.3. Variation of shear magnitude value on the Liutex core line with flow direction is shown in Fig. 7.3.

It can be seen that the $cos\theta$ value of Λ vortex leg begins to decrease in the middle and rear section, indicating that the inclined angle between Liutex and shear increases, and the shear value in the front section is greater than that in the middle and rear section (see Fig. 7.3). The shear magnitude value in the rear section of Λ vortex leg increases, while the cosine value decreases. Combined with the structural evolution of vortex in Fig. 7.4, it can be seen that the effect of shear in the rear section of Λ vortex leg affects the shape of vortex. An indication is that if the angle between Liutex and shear vectors in the vortex core is approximately zero, then this part of the vortex is more likely to be stable in the sense that the shape would basically remain the same. On the contrary, the vortex core where the angle is large tend to deform.

7.4.2.3 Comparison Between Different Times

In order to quantitatively study the change of the angle between Liutex and shear with different times and understand the interaction of Liutex and shear, we select five points on the Λ vortex core, and track the value of $cos\theta$ and shear magnitude at the same position but different time. The values are shown in Table 7.3. In addition, for the hairpin vortex, we select the maximum point of Liutex magnitude on the plane perpendicular to the y-axis as shown in Fig. 7.2b, and record the development of Liutex and shear on this particular point. It is found that on this point Liutex is approximately parallel to the shear. The time development of Liutex and shear magnitudes is listed in Table 7.5.

Λ vortex

We select five positions, which are $x_1 = 403.397\delta_{in}$, $x_2 = 406.396\delta_{in}$, $x_3 = 409.326\delta_{in}$, $x_5 = 412.349\delta_{in}$ and $x_6 = 415.397\delta_{in}$.

It can be seen that the structure of hairpin vortex is gradually generated at the rear end of Λ vortex leg in Fig. 7.4b. In Fig. 7.4c, the Λ vortex leg dissipates. Combined with Fig. 7.5, we find that the $cos\theta$ value of the front end (1cos, 2cos) of the leg is decreasing, the $cos\theta$ value of the middle and rear end (3cos, 4cos, 5cos) of the leg is increasing, and the angle between Liutex and shear is gradually decreasing.

It can be seen from the Fig. 7.6 that the closer to the rear end of the Λ vortex leg, the smaller the change value of shear with time. According to Fig. 7.4a, we find that

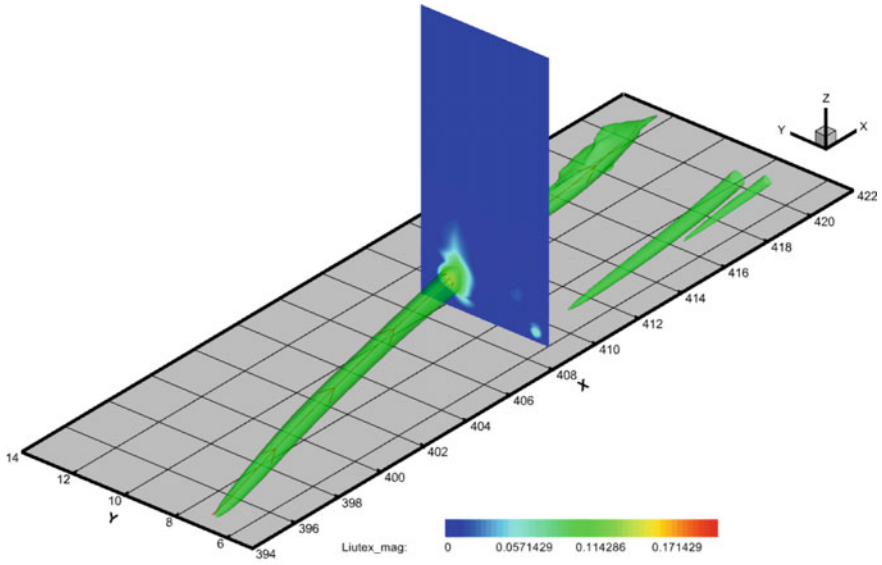

(a) vortex and slice at the position $X = 408.98$

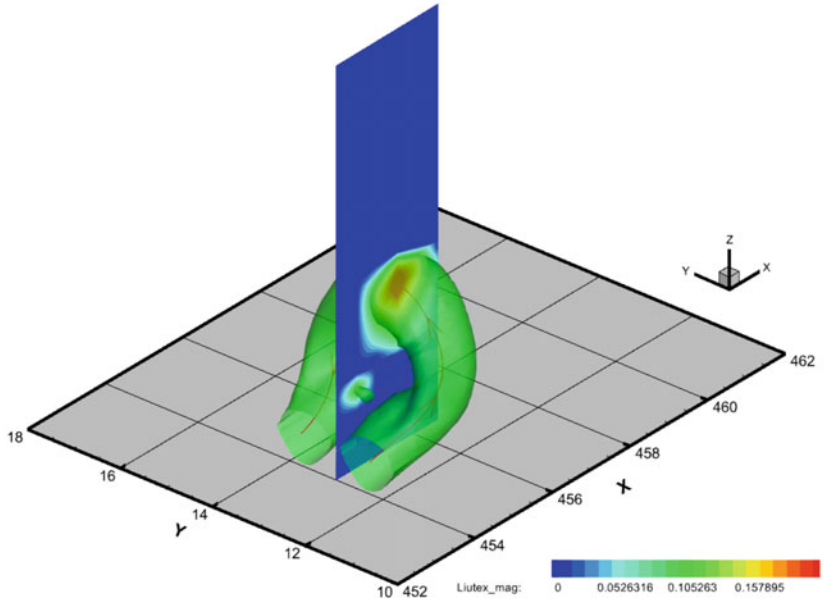

(b) Hairpin vortex and slice at the position $Y = 10.99$

Fig. 7.2 Λ vortex, hairpin vortex and Liutex lines ($t = 5.5T$)

Table 7.2 Distribution of Liutex, vorticity, shear magnitudes on the Λ vortex core ($t = 5.5T$)

X	Liutex_mag	Vorticity	Shear_mag	$cos\theta$
394.325	0.089	0.414	0.345	0.718
395.321	0.129	0.448	0.334	0.839
396.338	0.154	0.465	0.323	0.884
397.355	0.161	0.457	0.308	0.894
398.457	0.160	0.431	0.281	0.901
399.476	0.153	0.399	0.255	0.905
400.326	0.146	0.372	0.235	0.910
401.349	0.137	0.345	0.215	0.915
402.373	0.132	0.323	0.197	0.929
403.397	0.127	0.309	0.187	0.931
404.338	0.127	0.300	0.177	0.937
405.366	0.129	0.295	0.172	0.927
406.396	0.133	0.296	0.170	0.907
407.342	0.138	0.300	0.172	0.873
408.376	0.150	0.310	0.175	0.830
409.326	0.165	0.322	0.177	0.784
410.362	0.193	0.342	0.177	0.713
411.398	0.240	0.372	0.172	0.620
412.349	0.300	0.425	0.177	0.553
413.394	0.333	0.472	0.187	0.615
414.356	0.342	0.480	0.184	0.627
415.397	0.379	0.460	0.158	0.359
416.421	0.321	0.448	0.233	0.290
417.345	0.161	0.402	0.333	0.220

the shear value at the front end of the leg is relatively large and the evolution of Λ vortex structure of phase transition can be clearly seen (Figs. 7.4b and 7.4c).

Hairpin vortex

We select a hairpin vortex in the boundary layer transition process, extract the Liutex line data when $t = 5.5T$ (see in Table 7.4), and plot the value of $cos\theta$ varies with Y coordinate, as shown in the Fig. 7.7. It can be seen from the figure that the hairpin vortex is relatively stable, and the $cos\theta$ values on the vortex ring is between 0.93 and 1, indicating that the inclined angle between Liutex and shear at the vortex is quite small, and the angle at the highest part of the hairpin vortex is 0, with the highest point as the axis, and the $cos\theta$ values on both sides are very symmetrical (see Fig. 7.7).

It can be seen from Fig. 7.8 that the shear magnitude value and vorticity have the same change trend. The Liutex magnitude value, shear magnitude value, vorticity and $cos\theta$ value have good symmetry with respect to the section $Y = 10.99\delta_{in}$. The high

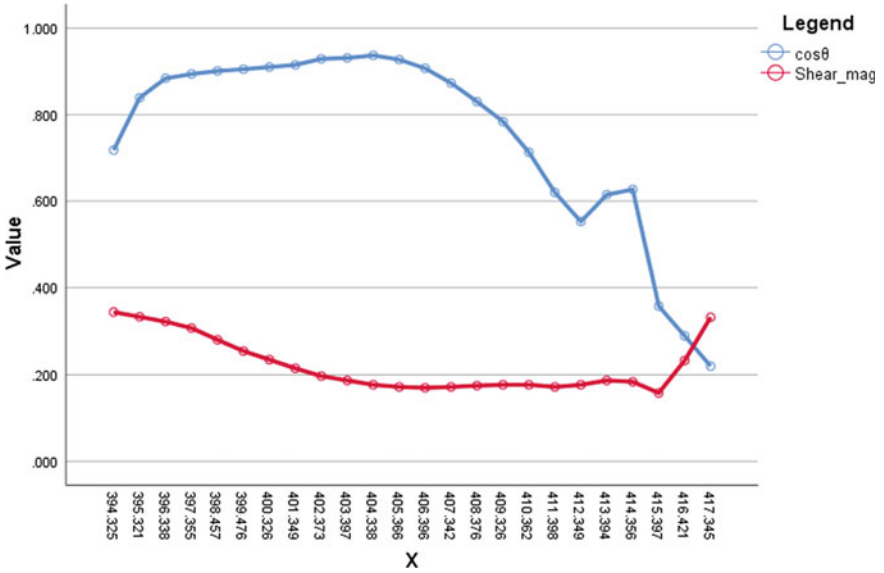

Fig. 7.3 The distribution of $cos\theta$ and shear magnitude on the Liutex core line of Λ vortex ($t = 5.5T$)

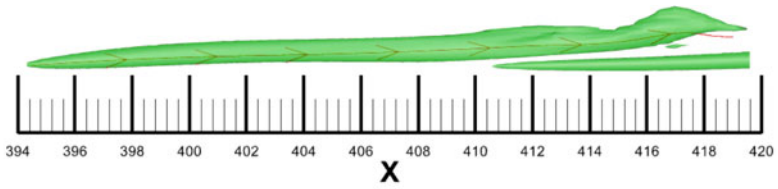

(a) $t = 5.5T$

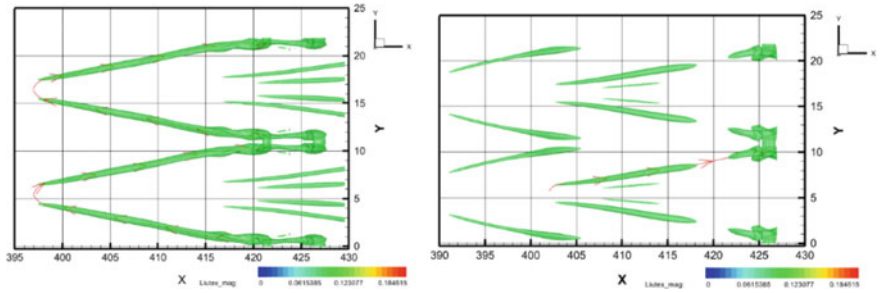

(b) $t = 5.75T$ (c) $t = 6.1T$

Fig. 7.4 The evolution of Λ vortex structure of transition (where T is the period of T-S wave)

Table 7.3 The value of $cos\theta$ and shear magnitude development at selected points

t	$T1 = 5.5T$	$T2 = 5.6T$	$T3 = 5.75T$	$T4 = 6.0T$	$T5 = 6.1T$
$cos\theta_1$	0.931	0.908	0.724	0.821	0.432
$cos\theta_2$	0.907	0.915	0.740	0.834	0.816
$cos\theta_3$	0.784	0.881	0.819	0.882	0.886
$cos\theta_4$	0.553	0.805	0.853	0.928	0.937
$cos\theta_5$	0.359	0.406	0.871	0.966	0.979
Shear_mag1	0.187	0.213	0.286	0.210	0.213
Shear_mag2	0.170	0.183	0.227	0.249	0.240
Shear_mag3	0.177	0.172	0.186	0.214	0.232
Shear_mag4	0.177	0.164	0.166	0.164	0.193
Shear_mag5	0.158	0.127	0.155	0.153	0.147

$cos\theta_{\#}$ represents the $cos\theta$ value of the #-th point, Shear_mag # represents the shear magnitude value of the #-th point. (# = 1, 2, 3, 4, 5)

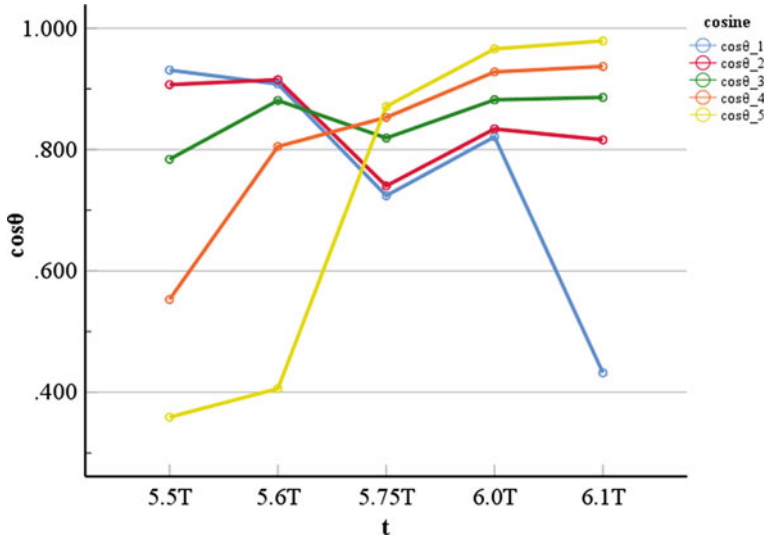

Fig. 7.5 The value of $cos\theta$ varies with five different times

shear value is mainly concentrated near the wall. The farther away from the wall, the smaller the shear magnitude value, and the Liutex magnitude value increases accordingly, but on the whole, the change range of Liutex magnitude value is far less than the shear value.

The above Fig. 7.9 shows the evolution of hairpin vortex structure of transition over time. Before $t = 6.1T$, the shape of hairpin vortex is relatively stable. When $t = 6.1T$ to $t = 6.3T$, the legs of hairpin vortex become thinner and fold inward,

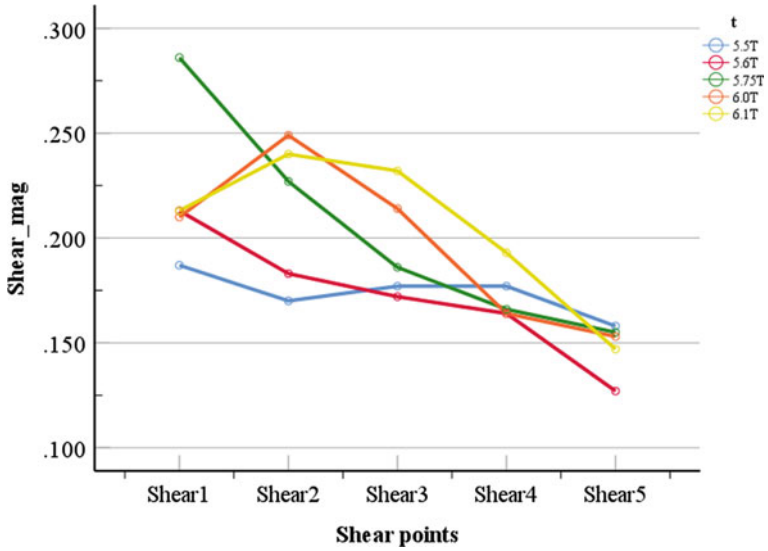

Fig. 7.6 The value of shear magnitude varies with five different times

and the integral mean value of $cos\theta$ decreases. After $t = 6.3T$, the legs of hairpin vortex begin to disappear and the shape becomes ring vortex. The integral average value of $cos\theta$ on the Liutex core line gradually increases, and the shear magnitude value at the maximum point of Liutex magnitude gradually decreases to 0 over time, while the size of Liutex magnitude is almost unchanged. As shown in Fig. 7.2b, at the different time, the $cos\theta$ values of the maximum Liutex magnitude at the slice at the position $Y = 10.99\delta_{in}$ are 1. According to the mathematical definition of vortex in the third-generation vortex identification method, the proportion of Liutex magnitude over vorticity can be analyzed since for the considered points they are in the same direction.

The proportion of Liutex magnitude in the hairpin vortex increases with time as shown in Fig. 7.10. When Liutex and shear vectors are approximately parallel, the vortex moves greatly along the flow direction and the offset in other directions is very small. Combined with Fig. 7.9, we can find that the hairpin vortex and the induced annular vortex are relatively stable.

7.5 Conclusion

According to the analysis of the specific vortices in the boundary layer transition, the following conclusions can be summarized.

Table 7.4 Distribution of Liutex, vorticity, shear magnitudes on a hairpin vortex core ($t = 5.5T$)

Y	Liutex_mag	Vorticity	Shear_mag	$cos\theta$
9.933	0.205	0.656	0.452	0.995
9.938	0.203	0.665	0.463	0.995
9.948	0.202	0.673	0.472	0.995
9.962	0.202	0.680	0.479	0.992
9.982	0.202	0.675	0.475	0.984
10.006	0.204	0.666	0.466	0.975
10.034	0.206	0.661	0.460	0.967
10.066	0.209	0.655	0.453	0.957
10.102	0.211	0.638	0.435	0.947
10.142	0.214	0.628	0.423	0.940
10.185	0.215	0.604	0.398	0.932
10.232	0.217	0.590	0.383	0.930
10.281	0.218	0.570	0.361	0.930
10.334	0.218	0.550	0.341	0.932
10.391	0.219	0.535	0.324	0.939
10.451	0.220	0.521	0.307	0.949
10.515	0.221	0.509	0.294	0.960
10.584	0.222	0.500	0.282	0.971
10.657	0.224	0.495	0.273	0.981
10.735	0.225	0.489	0.266	0.988
10.817	0.226	0.489	0.263	0.994
10.903	0.228	0.490	0.262	0.998
10.990	0.228	0.490	0.262	1.000
11.078	0.228	0.489	0.262	0.999
11.164	0.227	0.488	0.262	0.996
11.247	0.225	0.489	0.265	0.990
11.326	0.224	0.494	0.272	0.983
11.400	0.223	0.499	0.280	0.983
11.470	0.221	0.505	0.289	0.962
11.535	0.220	0.520	0.305	0.952
11.596	0.219	0.533	0.321	0.941
11.653	0.218	0.546	0.336	0.934
11.707	0.218	0.565	0.357	0.930
11.757	0.217	0.584	0.377	0.929
11.804	0.216	0.602	0.396	0.932
11.848	0.214	0.623	0.418	0.938

(continued)

Table 7.4 (continued)

Y	Liutex_mag	Vorticity	Shear_mag	$cos\theta$
11.889	0.211	0.633	0.430	0.945
11.926	0.209	0.650	0.447	0.955
11.959	0.207	0.662	0.460	0.965
11.988	0.204	0.666	0.465	0.973
12.013	0.203	0.673	0.473	0.982
12.033	0.202	0.682	0.481	0.991
12.049	0.201	0.674	0.473	0.994
12.060	0.202	0.666	0.465	0.996

Table 7.5 Liutex core line data at hairpin vortex core with times

t	Shear_mag	Liutex_mag	Vorticity	Percentage (%)	Integral average of $cos\theta$
5.5T	0.262	0.229	0.49	46.73	0.962
5.55T	0.225	0.208	0.433	48.04	0.946
5.6T	0.183	0.218	0.4	54.50	0.962
5.65T	0.172	0.207	0.379	54.62	0.961
5.7T	0.136	0.184	0.32	57.50	0.936
5.75T	0.141	0.186	0.324	57.41	0.941
5.8T	0.129	0.175	0.304	57.57	0.941
5.85T	0.14	0.159	0.299	53.18	0.939
5.9T	0.099	0.163	0.262	62.21	0.883
5.95T	0.099	0.163	0.263	61.98	0.85
6T	0.112	0.159	0.271	58.67	0.789
6.05T	0.113	0.153	0.265	57.74	0.747
6.1T	0.111	0.155	0.266	58.27	0.724
6.15T	0.104	0.159	0.263	60.46	0.680
6.2T	0.058	0.165	0.223	73.99	0.564
6.25T	0.057	0.174	0.231	75.32	0.428
6.3T	0.062	0.18	0.241	74.69	0.486
6.35T	0.069	0.183	0.252	72.62	0.643
6.4T	0.064	0.189	0.253	74.70	0.745
6.45T	0.057	0.192	0.249	77.11	0.750

1. Liutex can well capture vortices in boundary layer transition with its direction as the local rotational axis and magnitude as twice the angular velocity speed of local rotational motion.
2. Different from other vortex identification methods, Liutex is not contaminated by shear.

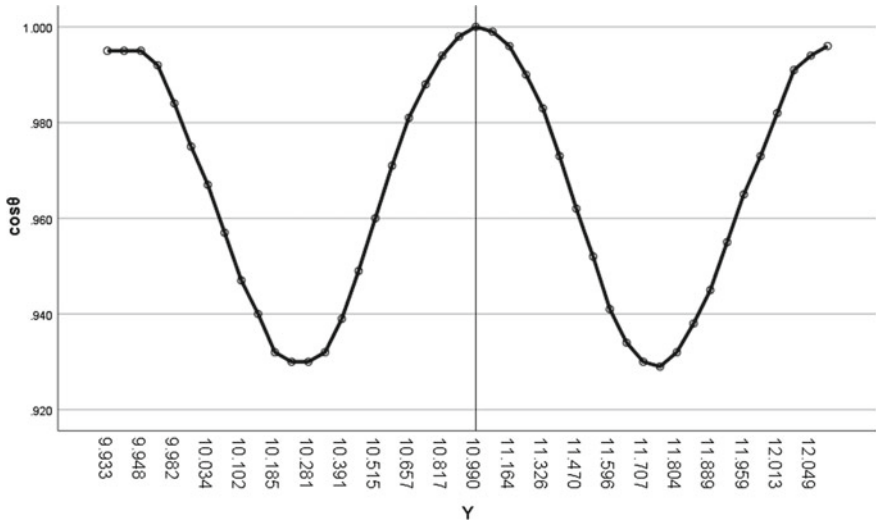

Fig. 7.7 The $cos\theta$ distribution on the Liutex core line of hairpin vortex ($t = 5.5T$)

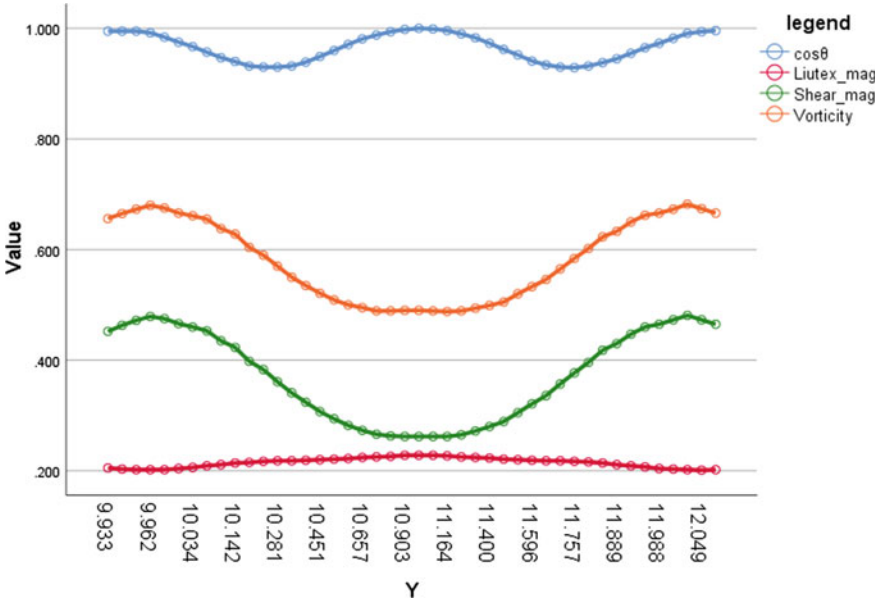

Fig. 7.8 The distribution of Liutex, vorticity, shear magnitudes on a hairpin vortex core ($t = 5.5T$)

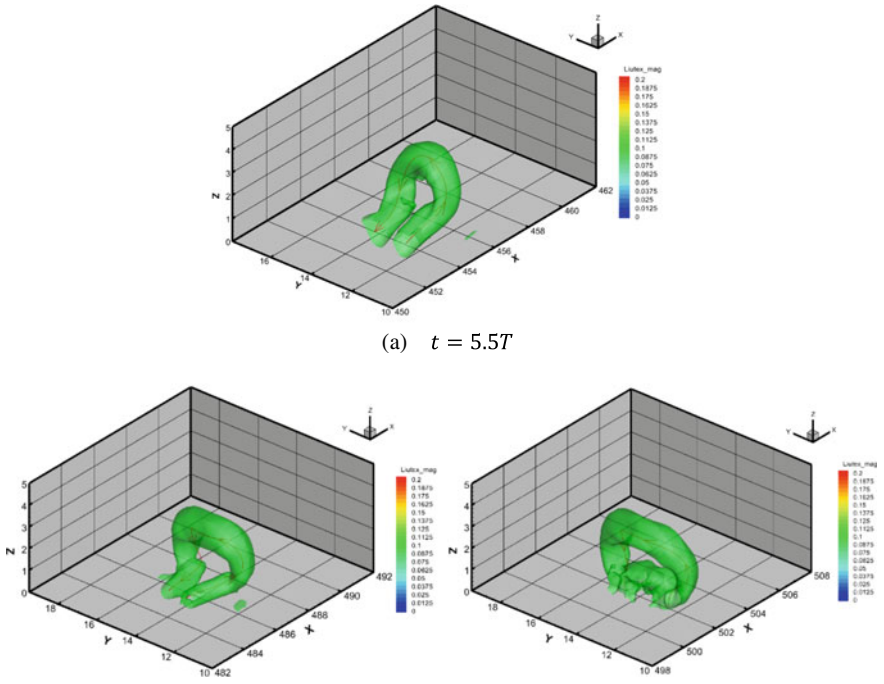

(a) $t = 5.5T$

(b) $t = 6.1T$ (c) $t = 6.4T$

Fig. 7.9 The evolution of hairpin vortex structure of transition (where T is the period of T-S wave)

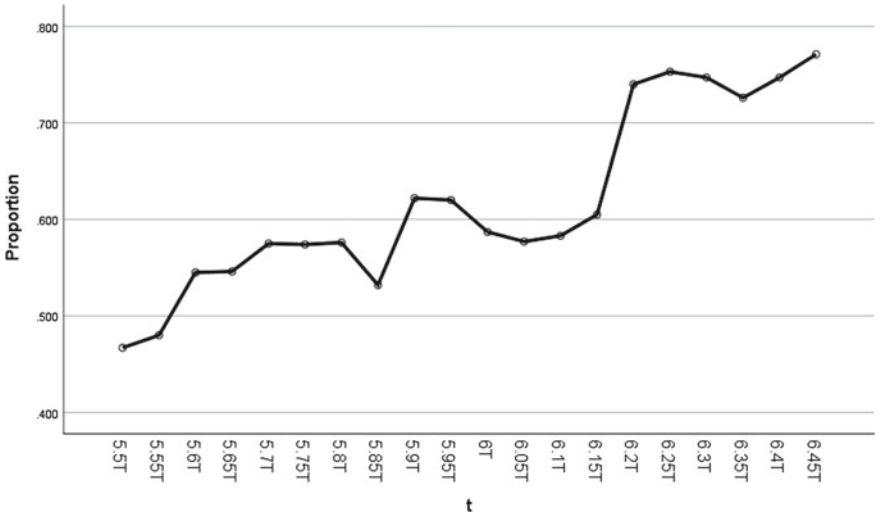

Fig. 7.10 The proportion of Liutex_mag/Vorticity varies with times

3. In the process of boundary layer transition, from the data, the inclined angle between Liutex and shear ranges from 0 to $\pi/2$. High shear is mainly concentrated before vortex generation and vortex dissipation, indicating that shear plays an important role in vortex formation and development.
4. Because of the Liutex shear interaction, Λ vortex gradually develops into hairpin vortex and some parts of it dissipates with time. At the same time, the hairpin vortex will generally maintain a stable state because the inclined angle between Liutex and shear is approximately zero, and then slowly become ring vortex. When the inclined angle between Liutex and shear is approximately parallel, the vortex mainly moves along the flow direction and the offset in other directions is very small.

References

1. C. Liu, Y. Yan, P. Lu, Physics of turbulence generation and sustenance in a boundary layer. J. Comput. Fluids. 353–384 (2014)
2. I.M. Wallace, Highlights from 50 years of turbulent boundary layer research. J. Turbul. 1–70 (2013)
3. S.K. Roblnson, Coherent motion in the turbulent boundary layer. J. Annu. Rev. Fluid. Mech. 601–639 (1991)
4. C. Liu, Y. Gao, X. Dong, et al., Third generation of vortex identification methods: Omega and Liutex/Rortex based systems. J. Hydrodyn. 205–223 (2019)
5. C. Liu, Y. Wang, Y. Yang, et al., New omega vortex identification metho. J. Sci. China. Phys. Mech. **59**(8) (2016)
6. C. Liu, Y. Gao, S. Tian, et al., Rortex-a new vortex vector definition and vorticity tensor and vector decompositions. J. Phys. Fluids. 30 (2018)
7. X. Dong, Y. Gao, C. Liu, New normalized Rortex/Vortex identification method. J. Phys. Fluids. 31 (2019)
8. Y. Wang, Y. Yang, G. Yang, et al., DNS study on vortex and vorticity in late boundary layer transition. J. Commu. Comput. Phys. 441–459 (2017)
9. C. Liu, Liutex-third generation of vortex definition and identification methods. J. Aerodyn. 413–431 (2020)
10. P. Shrestha, C. Nottage et al., Stretching and shearing contamination analysis for Liutex and other vortex identification methods. J. Aia. (2021). https://doi.org/10.1186/s42774-020-00060-9
11. Y. Wang, Y. Gao, J. Liu, et al., Explicit formula for the Liutex vector and physical meaning of vorticity based on the Liutex-Shear decomposition. J. Hydrodyn. 464–474 (2019)
12. Y. Yu, P. Shrestha, O. Alvarez, et al., Investigation of correlation between vorticity, Q, λci, λ2, Δ and Liutex. J. Comput. Fluids. 225 (2021)
13. X. Liu, L. Chen, C. Liu, Study of mechanism of ring-like vortex formation in late flow transition. J. AIAA 2010–1456 (2010)
14. P. Lu, C. Liu, Numerical study on mechanism of small vortex generation in boundary layer transition. J. AIAA 2011–2287 (2011)
15. F. Ducrous, P. Comte, M. Lesieur, Large-eddy simulation of transition to turbulence in a boundary layer developing spatially over a flat plate. J. Fluid. Mech. 1–36 (1996)
16. P. Lu, C. Liu, DNS study on mechanism of small length scale generation in late boundary layer transition. J. Phys. D 11–24 (2012)
17. P. Lu, M. Thapa, C. Liu, Numerical investigation on chaos in late boundary layer transition to turbulence. J. Comput. Fluids. 68–76 (2014).

18. H. Schlichting, K. Gersten, *Boundary Layer Theory*, 8th revised edn. (Springer, New York, 2000)
19. S. Bake, D. Meyer, U. Rist, Turbulence mechanism in Klebanoff transition: a quantitative comparison of experiment and direct numerical simulation. J. Fluid. Mech. 217–243 (2002)
20. L. Kleiser, T.A. Zang, Numerical simulation of transition in wall-bounded shear flows. J. Annu. Rev. Fluid. Mech. 495–537 (1991)
21. Y.S. Kachanov, in *Recent Results in Laminar-Turbulent Transition.* On a universal mechanism of turbulence production in wall shear flows, vol. 86 (Springer, Berlin, 2003), pp. 1–12
22. V.I. Borodulin, V.R. Gaponenko, Y.S. Kachanov, et al., Late-stage transition boundary-layer structure: direct numerical simulation and experiment. J. Theor. Comput. Fluid Dyn. 317–337 (2002)
23. W. Xu, Y. Wang, Y. Gao, et al., Liutex similarity in turbulent boundary layer. J. Hydrodyn. 1259–1262 (2019)
24. H. Guo, V.I. Borodulin, Y.S. Kachanov, C. Pan, J.J. Wang, X.Q. Lian, S.F. Wang, Nature of sweep and ejection events in transitional and turbulent boundary layers. J. Turbul. 1–51 (2010)
25. J. Cousteix, in *turbulence et couche limite.* Vol. 2, ed. by Cepadues, (Toulouse, Septembre, 1989), p. 627